Does clinical data quality affect fluid-structure interaction simulations of patient-specific stenotic aortic valve models?

Accepted manuscript at https://doi.org/10.1016/j.jbiomech.2019.07.047

Does clinical data quality affect fluid-structure interaction simulations of patient-specific stenotic aortic valve models?

Giulia Luraghi[a], Francesco Migliavacca[a], Claudio Chiastra[a,b], Alexia Rossi[c,d], Bernhard Reimers [d], Giulio G. Stefanini[c,d], Jose Felix Rodriguez Matas[a]

[a] Laboratory of Biological Structure Mechanics (LaBS), Department of Chemistry, Materials and Chemical Engineering "Giulio Natta", Milan, Italy.

[b] PoliTo*BIO*Med Lab, Department of Mechanical and Aerospace Engineering, Politecnico di Torino, Turin, Italy.

[c] Department of Biomedical Sciences, Humanitas University, Pieve Emanuele (MI), Italy.

[d] Cardio Center, Humanitas Clinical and Research Center - IRCCS, Rozzano (MI), Italy.

Corresponding author

Giulia Luraghi

Laboratory of Biological Structure Mechanics (LaBS), Department of Chemistry, Materials and Chemical Engineering "Giulio Natta", Piazza L. da Vinci 32, 20133 Milan, Italy.

giulia.luraghi@polimi.it

Abstract

Numerical models are increasingly used in the cardiovascular field to reproduce, study and improve devices and clinical treatments. The recent literature involves a number of patient-specific models replicating the transcatheter aortic valve implantation procedure, a minimally invasive treatment for high-risk patients with aortic diseases. The representation of the actual patient's condition with truthful anatomy, materials and working conditions is the first step toward the simulation of the clinical procedure.

The aim of this work is to quantify how the quality of routine clinical data, from which the patient-specific models are built, affects the outputs of the numerical models representing the pathological condition of stenotic aortic valve.

Seven fluid-structure interaction (FSI) simulations were performed, completed with a sensitivity analysis on patient-specific reconstructed geometries and boundary conditions. The structural parts of the models consisted of the aortic root, native tri-leaflets valve and calcifications. Ventricular and aortic pressure curves were applied to the fluid domain.

The differences between clinical data and numerical results for the aortic valve area were less than 2% but reached 12% when boundary conditions and geometries were changed. The difference in the aortic stenosis jet velocity between measured and simulated values was less than 11% reaching 27% when the geometry was changed. The CT slice thickness was found to be the most sensitive parameter on the presented FSI numerical model.

In conclusion, the results showed that the segmentation and reconstruction phases need to be carefully performed to obtain a truthful patient-specific domain to be used in FSI analyses.

Keywords: Fluid-Structure Interaction simulation (FSI), Aortic Valve, Patient-specific numerical models, Finite-Element Analysis (FEA)

Introduction

Numerical analysis is widely used to investigate cardiovascular biomechanics (Iaizzo, 2013). In particular, patient-specific models are used to reproduce human physiological and pathological conditions. In the *in silico* clinical trial arena, the fascination for "virtual" treatments and clinical procedure applied to "virtual" patients is gaining popularity in recent years. Similarly, in the personalized medicine area, patient-specific computational models are used for tailored therapies (Holmes and Lumens, 2018).

The recent literature indicates a number of examples of patient-specific aortic root models (Kalyana Sundaram et al., 2015; Spühler et al., 2018; Toma et al., 2016). The representation of the actual patient's condition with truthful anatomy, material, and working conditions is the first step toward the simulation of a clinical procedure like the Transcatheter Aortic Valve Implantation (TAVI) (Luraghi et al., 2019), which is a minimally invasive treatment for high-risk patients with aortic diseases including aortic stenosis (AS) (Smith et al., 2011). AS is one of the most common valvular pathology, which compromises the regulation of the blood flow between the left ventricle and the aorta. In patients with AS, the effective valve area is reduced due to calcifications; the resistance to the flow is increased together with the pressure drop (Baumgartner et al., 2009). The AS is classified in mild, moderate and severe according to the aortic valve area (AVA), with the mean pressure gradient across the valve and the peak velocity being estimated from a Doppler analysis (Baumgartner et al., 2009). Transthoracic Doppler echocardiography (TTE) is the main recommendation as a primary imaging modality to assess stenosis (Kappetein et al., 2012) and to evaluate the AVA with the continuity equation. It was demonstrated (Halpern et al., 2009; Kempfert et al., 2012) that TTE underestimates the AVA with respect to the planimetered AVA estimated with multidetector computed tomography (CT) (Le Couteulx et al., 2018; O'Brien et al., 2011) or Magnetic Resonance Imaging (MRI) (Chun et al., 2008). This is due primarily to the assumption of the circular Left Ventricular

Outflow Tract (LVOT) in the calculation of AVA with the continuity equation. Nowadays, it is well known that CT images should be a fully integrated component on any TAVI program (Blanke et al., 2019).

The success of the TAVI procedure is conditioned by a proper "sizing" estimation (Kasel et al., 2013), namely the correct choice of available valve sizes according to the size of the native aortic annulus. A correct measurement of the aortic annulus is therefore mandatory to prevent post-implantation complications (Lehmkuhl et al., 2013), as has been demonstrated by both *in vitro* (Dasi et al., 2017; Maleki et al., 2015) and *in silico* (Abbasi and Azadani, 2015; Born et al., 2014) models. Undersizing or oversizing of the valve annulus may lead to important complications as paravalvular leakage (Jilaihawi et al., 2012; Kim et al., 2018). In this regard, a combination of 2-dimensional and 3-dimensional (3D) TTE with CT or MRI exams (Delgado et al., 2010; Jánosi et al., 2011) can improve the accuracy of the annulus diameter estimation. Moreover, also in relation to imaging, CT scans are often used to segment and reconstruct TAVI patient-specific domains (Bailey et al., 2017; Basri et al., 2016; Bianchi et al., 2016; Bosi et al., 2018; Bosmans et al., 2016; Cabrera et al., 2017; Capelli et al., 2012; El Faquir et al., 2017; Gunning et al., 2015; Kandail et al., 2018; Kopanidis et al., 2015; Mao et al., 2018; Ovcharenko et al., 2016; Russ et al., 2013; Wu et al., 2016b). Consensus regarding aortic root reconstruction recommends the use of multidetector CT system with a spatial resolution between 0.5 to 0.6 mm (Holmes et al., 2012; Schoenhagen et al., 2010) as reported in a few numerical studies (Bianchi et al., 2016; Bosmans et al., 2016; Hasan et al., 2017; Kopanidis et al., 2015). However, how the CT spatial resolution influences the results of a numerical patient-specific FSI simulation has not yet been investigated.

Necessary elements in a pre-TAVI stenotic patient specific model are the boundary conditions. In this regard, the patient's pressure tracings are important clinical data necessary to set up a numerical model. However, recorded pressure tracings including the actual pressure curves for

both the ventricular and aortic sides are rare in clinical procedures, with clinical information usually limited to values of the minimum and maximum pressure and the heart rate, without including the original waveforms. For these reasons, in most patient-specific simulation studies, boundary conditions are set in terms of inlet and outlet pressures, with the applied pressure curves being idealized (Mao et al., 2018; Sturla et al., 2013; Wu et al., 2016b) or estimated using lumped-parameter models (Kandail et al., 2018). In some cases, however, a combination of flow and pressure boundary conditions is used (Kalyana Sundaram et al., 2015). The aim of this work is to estimate by means of fluid-structure interaction (FSI) simulations, which represent the best numerical approach to investigate the biomechanics of heart valves (Luraghi et al., 2017), how the quality of clinical data affects the numerical results of patient-specific stenotic aortic valve analyses. In particular, this work focuses on the importance of reconstructing truthful and accurate pre-TAVI stenotic patient-specific models from clinical data as a first step towards a model for predicting the efficacy of TAVI in recovering normal valvular function and hemodynamics. The main hypothesis is that the quality of the clinical data used to set-up an FSI patient-specific model has an impact on the numerical outputs and the subsequent conclusions derived from the analysis. In particular, 7 patients with different clinical data i.e., CT spatial resolution and pressure data, were investigated. In terms of CT spatial resolution, images were acquired with a slice thickness of 0.6 mm for 5 patients, whereas for two patients the axial resolution was of 3 mm. In terms of pressure data, the full pressure tracings were present only for one patient whereas for the remaining patients only the systolic and diastolic pressures were available. This study wants to enlighten the importance to develop realistic and accurate FSI patient-specific models that might be used as support for surgical planning before the implantation of a transcatheter valve.

Materials and Methods

Clinical Data

Data from 7 patients (cases from A to G) with a severe level of aortic stenosis who underwent TAVI were analyzed retrospectively. The study complies with the Declaration of Helsinki on human research. All the patients were included in a prospective registry, approved by the Institutional ethics committee, and gave written informed consent.

Preoperative assessment by means of TTE (EPIQ 7C Philips Medical System. Philips Healthcare, Best, The Netherlands) acquired at a plane coincident with the coronary sinuses (downstream the valvular plane) confirmed the severity of the AS by estimating the AS jet velocity, the mean pressure gradient and the AVA (Baumgartner et al., 2009).

AS jet velocity, directly measured from the continuous-wave TTE is the antegrade systolic velocity across the narrowed aortic valve. It is defined as the highest velocity obtained from any considered window. The transvalvular aortic gradient in systole was calculated from the velocity (v) using Bernoulli's equation as:

$$\Delta P = 4v^2 \tag{1}$$

The AVA was estimated based on the continuity equation as follows:

$$AVA = \frac{CSA_{LVOT} \cdot VTI_{LVOT}}{VTI_{AV}} \tag{2}$$

$$CSA_{LVOT} = \pi \left(\frac{D}{2}\right)^2 \tag{3}$$

where D is the diameter of the LVOT, VTI_{LVOT} and VTI_{AV} are the velocity time integral upstream and downstream the aortic valve respectively calculated from the recorded pulsed-wave TTE, and CSA_{LVOT} is the cross-sectional area of the LVOT. Table 1 reports these

parameters for the 7 investigated patients. The AVA estimated from TTE measures is known also as effective orifice area (EOA). On the contrary, the geometric orifice area (GOA) is planimetrically measured from multidetector CT or MRI (Garcia and Kadem, 2006). Based on these parameters, the contraction coefficient C_c is computed as:

$$C_c = \frac{EOA}{GOA} \tag{4}$$

This coefficient can reach a value of 0.7 for severe stenotic patients (de la Fuente Galán et al., 1996).

CT scans with two machines with different spatial resolution were regularly performed prior TAVI. Table 2 reports the CT spatial resolution for each patient. In particular, the acquisitions with a slice thickness of 3.0 mm were performed with the Philips Brilliance 16-Slice CT scanner (Philips Healthcare, Best, The Netherlands), while those with a slice thickness of 0.6 mm with the GE Medical System Revolution EVO CT scanner (GE Medical System, Chicago, IL, USA). The aortic valve annuli were estimated through TTE in terms of long and short diameter, or directly from the CT scans (Blanke et al., 2019; Kasel et al., 2013), as reported in Table 2.

Invasive aortic and ventricular pressure data were collected before TAVI for each patient, in terms of maximum and minimum (telediastolic) values and heart rate. Full pressure tracings, were available only for patient B. Table 3 summarizes pressures and heart rate for the remaining 7 patients under consideration.

FSI Model

The CT scans of the 7 patients were processed with Mimics (Materialise, Leuven, Belgium) to reconstruct the 3D patient-specific domains. The CT images were segmented semi-

automatically using grey-value thresholding followed by morphologic operations (Fig. 1 left-top panel). In particular, for the aortic lumen, the range threshold for segmentation was set as 50-560 HU, following by a dynamic region growing algorithm, opening operator and a few multiple slice editor operations. The aortic lumen was smoothed by keeping the volume loss under 2% and the cut from the LVOT to the mid-ascending aorta. For the calcifications, the range threshold was set >600 and the relative mask was obtained with a smoothing operation by keeping the volume loss under 8%.

The obtained segmented masks were then used to derive triangulated meshes representing the 3D models of the aortic root and the calcium deposits. The surface lumen (Fig. 2a) of the aorta was extruded in the radial direction to obtain a constant thickness of 2 mm (Capelli et al., 2012). The aortic vessel was discretized with hexahedral tri-linear fully integrated solid elements with an average element size of 1 mm and three elements through its thickness (Fig. 2b). The native valves were generated by following reference points identified at the commissural ends and basal leaflet attachment lines on the aortic lumen (Morganti et al., 2014). Three drawn lines identified each of the three leaflets of the valve and three surfaces were constructed in ANSA Pre Processor v19.0 (BETA CAE Systems, Switzerland) by defining the free margin as a circular arc (Fig. 2c). The main dimensions of the native valves result in line with values from literature (Haj-Ali et al., 2012). The valves were discretized with Belytschko-Lin-Tsay quadrilateral bi-linear shell elements with one-point integration (Fig. 2d) and viscosity hourglass control (Luraghi et al., 2018). The thickness of the native valves was set to 0.5 mm (Capelli et al., 2012; Ranga et al., 2004). A pre-analysis was performed to obtain the end-diastole close configuration of the valves (Fig. 2e), by directly applying the pressure gradient. The smoothed segmented calcium deposits were discretized with tetrahedral elements. All meshes were created with ANSA Pre Processor v19.0 (BETA CAE Systems, Switzerland).

Sensitivity analysis of the mesh size was performed in a previous work of ours (Luraghi et al., 2018). The whole set of patient-specific models (from A to G) are shown in Fig. 1.

The aortic tissue was modeled as an anisotropic hyperelastic material with two preferred directions coinciding with the longitudinal and circumferential directions. Experimental biaxial data from healthy abdominal aorta was considered (Vande Geest et al., 2006). The native valves and calcifications were modeled as linear elastic materials with a density of 1100 kg/m^3, Young's modulus of 4 MPa and Poisson's ratio of 0.45 (Vy et al., 2016) for the valve and a density of 2000 kg/m^3, Young's modulus of 12.6 MPa and Poisson's ratio of 0.45 (Holzapfel et al., 2004) for the calcifications, respectively. Node-to-surface tied contacts were defined between the commissural edges of the native valves and the internal surface of the aorta, whereas surface-to-surface tied contacts were defined between the calcifications and the leaflets (Fig. 2f). As boundary conditions, both ends of the aorta were fixed in all directions.

The "operator split" Lagrangian-Eulerian approach (Benson, 1992), a non-boundary fitted method implemented in the solver LS-DYNA 971 R10.0 (LSTC, Livermore, CA. USA), was adopted to define the FSI problem. Fluid domains, in which all the structures of the models were immersed, were created and discretized with 1 mm hexahedral elements (Luraghi et al., 2018). Blood was modeled as a Newtonian fluid, with a density of 1060 kg/m^3 and a dynamic viscosity of 3.5 cP. Aortic and ventricular pressure curves were imposed as boundary conditions to the outlet and inlet surfaces of the fluid domains (Fig. 3). Since actual pressure curves were available only for patient B (Fig. 3), for the remaining patients a physiological waveform was scaled to match the available patient's maximum and minimum pressure values. Figure 4 shows the scaled physiological waveform for patient B (dotted curves). Two cardiac cycles were simulated and results from the second cycle were considered.

Results

Aortic Annular Sizing

A quantitative comparison between the equivalent clinical measurements of the aortic annulus and the segmented ones was performed and reported in Table 4. In particular, the reconstructed annuli were measured as the diameter of the circumference passing through the three anchor points at the attachment edge, according to the definition of valve annulus i.e., the virtual ring obtained by joining three basal attachment points of the aortic leaflets (Kasel et al., 2013). In general, the annulus size measured from segmentation was higher than the average value computed in clinic (Table 4). The percentage differences between the clinical and model annulus size obtained for each patient were 6% (patient A), 0% (patient B), 34% (patient C), 19% (patient D), 21% (patient E), 52% (patient F) and 4% (patient G).

Aortic valve area

GOA values from the FSI results were obtained by post-processing the peak-systolic frame, shown in Fig. 5. In particular, the free margin of the three leaflets was projected on a plane parallel to the annulus and the resulted area was calculated. For comparison purposes, the clinical EOAs reported in Table 1 were rewritten as GOAs using Eq. (4) with a C_c of 0.7 (de la Fuente Galán et al., 1996). The percentage difference between the clinical and the model GOA was lower than 10% for all the patients, namely, 4% (patient A), 1% (patient B), 9% (patient C), 6% (patient D), 6% (patient E), 6% (patient F) and 1% (patient G).

Aortic stenosis jet velocity

Velocity field obtained at the systolic peak from FSI simulations for each patient was compared with the jet velocity measured from the continuous-wave Doppler ultrasound (Fig. 5). In all cases, the numerical jet velocity was lower than the value measured in clinic, as shown in Table

4. The percentage difference for each patient was -17% (patient A), -8% (patient B), -39% (patient C), -9% (patient D), -20% (patient E), -6% (patient F) and -12% (patient G).

Sensitivity analysis of clinical data

The previous results seem to indicate a significant influence of the quality of the clinical data on the aortic annular sizing and the AS jet velocity, with differences up to 52% and 39% respectively, relative to the difference between clinical and numerical data. Therefore, in order to asses the influence of the quality of the clinical data on the numerical results, a sensitivity analysis of the quality of the imaging clinical data was performed. The study was performed on patient B because a high spatial resolution CT scan and the pressure traces were available for this case. Therefore, two additional models were created from this patient. The first model, model $B_{pressure}$, aimed at investigating the impact of different pressure curve waveforms as boundary conditions of the FSI model. In this regard, physiological waveforms scaled to match the patient's maximum and minimum pressure values were applied instead of the patient-specific waveforms (see Fig. 4). The second model, model B_{CT}, was created to investigate how the spatial resolution, in particular, the slice thickness of the CT scan, influences the reconstructed geometry, and consequently the FSI simulation. In this regard, the original CT images of patient B were decimated by removing three slices out of four, resulting in a slice thickness of 2.4 mm. The geometry was reconstructed from scratch. Figure 4 shows a comparison between the geometries obtained from the original and decimated CT scans for patient B. It is worth noting that the increase of the CT slice thickness in patient B (case B_{CT}) resulted in a smaller annulus size (9% difference) with respect to the high-resolution image based model. Regarding the aortic valve area, the differences for the $B_{pressure}$ and B_{CT} with respect to the original model B_2 were 2% and 14% respectively. All values of GOA calculated from clinical and modeling data are reported in Table 4. Finally, for the AS jet velocity, the

modified models $B_{pressure}$ and B_{CT} underestimated the value with respect to the original B_2 model by -11% and -27% respectively.

Discussion

Building a reliable patient-specific model is the first step toward a robust numerical framework to study devices and clinical interventions. TAVI is characterized by the presence of calcium deposits on the native tri-leaflets valves, high-pressure gradient, and high jet velocity (Baumgartner et al., 2009). In this study, CT images and pressure data collected for 7 patients in the pre-TAVI phase were used. Previous works reported spatial resolution for CT images between 0.5 and 0.6 mm as optimum for generating patient-specific models (Holmes et al., 2012; Schoenhagen et al., 2010). In fact, in the few patient-specific studies on TAVI found in the literature where the spatial resolutions of the CT scans were explicitly reported, it was of 0.5 or 0.6 mm (Bianchi et al., 2016; Bosmans et al., 2016; Hasan et al., 2017; Kopanidis et al., 2015). Furthermore, it is uncommon in patient-specific models to apply as boundary conditions the actual patient's pressure curves. This is due to the fact that available clinical data is usually restricted to the systolic and diastolic pressure values. In this regard, idealized pressure curves (Mao et al., 2018; Sturla et al., 2013; Wu et al., 2016) or estimated from mathematical studies (Kandail et al., 2018) are usually applied as boundary conditions in the simulations.

Seven patients affected by severe AS were modeled and their pathological conditions were efficaciously described, in agreement with clinical data. A sensitivity analysis was conducted on one patient (patient B) for which high-resolution CT scan and full pressure tracings were available. The difference between clinical data and numerical results were calculated in terms of geometrical (i.e. aortic annular sizing), kinematic (i.e. aortic valve area), and fluid dynamic (i.e. aortic stenosis jet velocity) features.

To the best of our knowledge, this is the first study in which the impact of these parameters on the patient-specific reconstructed 3D domain and on the resulting fluid-structure simulations is investigated. In particular, the considered FSI methodology allows to quantify how changes in the boundary conditions on the fluid domain (pressure waveforms) affect the valve kinematics, and how changes on the morphology of the vessel (due to low-resolution CT image) and calcifications affect the hemodynamics.

Aortic annular sizing comparison showed that the clinical measurements from TTE and CT were in general smaller than annular sizing obtained from segmented images. It is in part due to differences in the methodology used to measure the annulus based on TTE and CT in clinic which are based on one or two planes, whereas the size obtained from segmented images is based on the entire valvular plane and is considered to be more precise. However, the percentage differences were found to be less than 20% for those patients with a CT scan resolution of 0.6 mm, whereas for those patients with a CT scan resolution of 3 mm the differences exceeded 30%. These results are in agreement with previous studies (Holmes et al., 2012; Schoenhagen et al., 2010). This observation was further corroborated by the sensitivity analysis conducted on patient B for which the difference in the anulus size between model B and model B_{CT} was of 9% (model B_{CT} underestimates the anulus size with respect to model B). Regarding the aortic stenosis jet velocity, simulations always underestimated the clinical value, with no particular differences observed for those patients associated with a CT scan with better resolution. The sensitivity analysis performed on patient B did not show a significant impact of the pressure curve on the simulation results (8% difference for the true pressure waveform against 11% difference for the idealized pressure waveform). However, results were more sensitive to the CT scan resolution as 27% difference against 8% difference was found for the cases with fine and lower resolution, respectively. These results suggest that the CT slice thickness (i.e. the CT scan axial space resolution) is the most sensitive parameter on the FSI

simulations in great part due to the impact that CT scan resolution has on the reconstructed geometry. However, underestimation of the jet velocity by the numerical solution can also be associated with the non-boundary fitted method used for the simulations. In the implementation of the method within LS-DYNA, a fixed cartesian mesh is used to discretize the fluid domain i.e, a fitted fluid mesh is not used around the leaflets. This implies that the fluid dynamic field near the leaflets is not adequately approximated leading to underestimating the peak velocity during systole. However, an intrinsic advantage of the numerical model is the quantification of the stress fields on the aorta, valves, and calcifications obtained from the FSI simulations. Although the stress field is not used for validation purpose, it could be of relevance when studying the consequences of TAVI in patients. In fact it is well know that one complication after TAVI could be the vascular damage (Jung et al., 2017).

This work is not absent of limitations. Tissue material properties are not patient-specific, and a sensitivity analysis will be required. However, our experience suggests lower variations associated with patient-specific vessel material in comparison to variations associated with patient-specific geometries and boundary conditions. On the contrary, hyperelastic models for the valve leaflets and elastoplastic model for the calcifications need further investigation. In this work, we have assumed constant thickness for the aorta and the native valve leaflets. In addition, the valve has been delineated from reference points of the patient-specific aorta because it was not possible to segment the native leaflets. It is true that considering a variable leaflet thickness (i.e. thickness reducing in the radial direction) may lead to larger values of the GOA and a reduction in the SA jet velocity. However, this truly patient-specific parameter cannot be uniquely determined from CT and Doppler data; therefore, assuming a real thickness variation represents an additional uncertainty that may result more difficult to quantify than the case of constant thickness. However, based on the results of this work, prospective collection of different CT machine scans and different CT acquisition protocols could be performed. In

conclusion, the development of realistic and accurate FSI patient-specific models can be used as support for clinical decisions before the device implantation. Numerical models provide complementary details that clinical data are usually lacking, as three-dimensional annulus geometry and fluid dynamics details. The use of a patient-specific geometry and boundary conditions allows taking into account the different features of each patient. The main hypothesis of this work, the quality of the clinical data used to set an FSI patient-specific model has an impact on the numerical outputs and the subsequent conclusions derived from this analysis was demonstrated. The developed model can be used to simulate the implantation of the transcatheter aortic valve and could help clinicians to predict the behavior of the prosthesis once implanted. In particular, the implantation procedure could be investigated and optimized in severe stenosis-affected virtual patients.

Acknowledgments: The authors thank Arianna Bianchi and Eva Legramandi for their precious contribution to the 3D reconstructions and simulations.

Conflict of interest: none

References

Abbasi, M., Azadani, A.N., 2015. Leaflet stress and strain distributions following incomplete transcatheter aortic valve expansion. J. Biomech. 48, 3663–3671. https://doi.org/10.1016/j.jbiomech.2015.08.012

Bailey, J., Curzen, N., Bressloff, N.W., 2017. The impact of imperfect frame deployment and rotational orientation on stress within the prosthetic leaflets during transcatheter aortic valve implantation. J. Biomech. 53, 22–28. https://doi.org/10.1016/j.jbiomech.2016.12.031

Basri, A.A., Zuber, M., Zakaria, M.S., Basri, E.I., Aziz, A.F.A., Ali, R.M., Tamagawa, M., Ahmad, K.A., 2016. The Hemodynamic Effects of Paravalvular Leakage Using Fluid

Structure Interaction; Transcatheter Aortic Valve Implantation Patient. J. Med. Imaging Heal. Informatics 6, 1513–1518. https://doi.org/10.1166/jmihi.2016.1840

Baumgartner, H., Hung, J., Bermejo, J., Chambers, J.B., Evangelista, A., Griffin, B.P., Iung, B., Otto, C.M., Pellikka, P.A., Quiñones, M., American Society of Echocardiography, European Association of Echocardiography, 2009. Echocardiographic Assessment of Valve Stenosis: EAE/ASE Recommendations for Clinical Practice. J. Am. Soc. Echocardiogr. 22, 1–23. https://doi.org/10.1016/j.echo.2008.11.029

Benson, D.J., 1992. Computational methods in Lagrangian and Eulerian hydrocodes. Comput. Methods Appl. Mech. Eng. 99, 235–394. https://doi.org/10.1016/0045-7825(92)90042-I

Bianchi, M., Marom, G., Ghosh, R.P., Fernandez, H.A., Taylor, J.R., Slepian, M.J., Bluestein, D., 2016. Effect of Balloon-Expandable Transcatheter Aortic Valve Replacement Positioning: A Patient-Specific Numerical Model. Artif. Organs 40, E292–E304. https://doi.org/10.1111/aor.12806

Blanke, P., Weir-McCall, J.R., Achenbach, S., Delgado, V., Hausleiter, J., Jilaihawi, H., Marwan, M., Norgaard, B.L., Piazza, N., Schoenhagen, P., Leipsic, J.A., 2019. Computed tomography imaging in the context of transcatheter aortic valve implantation (TAVI) / transcatheter aortic valve replacement (TAVR): An expert consensus document of the Society of Cardiovascular Computed Tomography. J. Cardiovasc. Comput. Tomogr. 13, 1–20. https://doi.org/10.1016/j.jcct.2018.11.008

Born, S., Sundermann, S.H., Russ, C., Hopf, R., Ruiz, C.E., Falk, V., Gessat, M., 2014. Stent Maps — Comparative Visualization for the Prediction of Adverse Events of Transcatheter Aortic Valve Implantations. IEEE Trans. Vis. Comput. Graph. 20, 2704–2713. https://doi.org/10.1109/TVCG.2014.2346459

Bosi, G.M., Capelli, C., Cheang, M.H., Delahunty, N., Mullen, M., Taylor, A.M., Schievano,

S., 2018. Population-specific material properties of the implantation site for transcatheter aortic valve replacement finite element simulations. J. Biomech. 71, 236–244. https://doi.org/10.1016/j.jbiomech.2018.02.017

Bosmans, B., Famaey, N., Verhoelst, E., Bosmans, J., Vander Sloten, J., 2016. A validated methodology for patient specific computational modeling of self-expandable transcatheter aortic valve implantation. J. Biomech. 49, 2824–2830. https://doi.org/10.1016/j.jbiomech.2016.06.024

Cabrera, M.S., Oomens, C.W.J., Baaijens, F.P.T., 2017. Understanding the requirements of self-expandable stents for heart valve replacement: Radial force, hoop force and equilibrium. J. Mech. Behav. Biomed. Mater. 68, 252–264. https://doi.org/10.1016/j.jmbbm.2017.02.006

Capelli, C., Bosi, G.M., Cerri, E., Nordmeyer, J., Odenwald, T., Bonhoeffer, P., Migliavacca, F., Taylor, A.M., Schievano, S., 2012. Patient-specific simulations of transcatheter aortic valve stent implantation. Med. Biol. Eng. Comput. 50, 183–192. https://doi.org/10.1007/s11517-012-0864-1

Chun, E.J., Choi, S. Il, Lim, C., Park, K.-H., Chang, H.-J., Choi, D.-J., Kim, D.H., Lee, W., Park, J.H., 2008. Aortic Stenosis: Evaluation with Multidetector CT Angiography and MR Imaging. Korean J. Radiol. 9, 439. https://doi.org/10.3348/kjr.2008.9.5.439

Dasi, L.P., Hatoum, H., Kheradvar, A., Zareian, R., Alavi, S.H., Sun, W., Martin, C., Pham, T., Wang, Q., Midha, P.A., Raghav, V., Yoganathan, A.P., 2017. On the Mechanics of Transcatheter Aortic Valve Replacement. Ann. Biomed. Eng. 45, 310–331. https://doi.org/10.1007/s10439-016-1759-3

de la Fuente Galán, L., San Román Calvar, J.A., Muñoz San José, J.C., Vega Barbado, J.L., del Pozo Crespo, F., Martín, J.A., Durán Hernández, J.M., Gimeno de Carlos, F., Fernández-Avilés, F., 1996. Influence of the degree of aortic valve calcification on the

estimate of valvular area using planimetry with transesophageal echocardiography. Rev. Esp. Cardiol. 49, 663–8.

Delgado, V., Schuijf, J.D., Bax, J.J., 2010. Pre-operative aortic valve implantation evaluation: multimodality imaging. EuroIntervention 6 Suppl G, G38-47. https://doi.org/10.4244/

El Faquir, N., Ren, B., Van Mieghem, N.M., Bosmans, J., De Jaegere, P.P., 2017. Patient-specific computer modelling - its role in the planning of transcatheter aortic valve implantation. Neth. Heart J. 25, 100–105. https://doi.org/10.1007/s12471-016-0923-6

Garcia, D., Kadem, L., 2006. What do you mean by aortic valve area: geometric orifice area, effective orifice area, or gorlin area? J. Heart Valve Dis. 15, 601–8.

Gunning, P.S., Saikrishnan, N., Yoganathan, A.P., McNamara, L.M., 2015. Total ellipse of the heart valve: the impact of eccentric stent distortion on the regional dynamic deformation of pericardial tissue leaflets of a transcatheter aortic valve replacement. J. R. Soc. Interface. https://doi.org/10.1098/rsif.2015.0737

Haj-Ali, R., Marom, G., Ben Zekry, S., Rosenfeld, M., Raanani, E., 2012. A general three-dimensional parametric geometry of the native aortic valve and root for biomechanical modeling. J. Biomech. 45, 2392–2397. https://doi.org/10.1016/j.jbiomech.2012.07.017

Halpern, E.J., Mallya, R., Sewell, M., Shulman, M., Zwas, D.R., 2009. Differences in Aortic Valve Area Measured with CT Planimetry and Echocardiography (Continuity Equation) Are Related to Divergent Estimates of Left Ventricular Outflow Tract Area. Am. J. Roentgenol. 192, 1668–1673. https://doi.org/10.2214/AJR.08.1986

Hasan, A., Kolahdouz, E.M., Enquobahrie, A., Caranasos, T.G., Vavalle, J.P., Griffith, B.E., 2017. Image-based immersed boundary model of the aortic root. Med. Eng. Phys. 47, 72–84. https://doi.org/10.1016/J.MEDENGPHY.2017.05.007

Holmes, D.R., Mack, M.J., Kaul, S., Agnihotri, A., Alexander, K.P., Bailey, S.R., Calhoon, J.H., Carabello, B.A., Desai, M.Y., Edwards, F.H., Francis, G.S., Gardner, T.J.,

Kappetein, A.P., Linderbaum, J.A., Mukherjee, C., Mukherjee, D., Otto, C.M., Ruiz, C.E., Sacco, R.L., Smith, D., Thomas, J.D., 2012. 2012 ACCF/AATS/SCAI/STS Expert Consensus Document on Transcatheter Aortic Valve Replacement. J. Am. Coll. Cardiol. 59, 1200–1254. https://doi.org/10.1016/J.JACC.2012.01.001

Holmes, J.W., Lumens, J., 2018. Clinical Applications of Patient-Specific Models: The Case for a Simple Approach. J. Cardiovasc. Transl. Res. 11, 71–79. https://doi.org/10.1007/s12265-018-9787-z

Holzapfel, G.A., Sommer, G., Regitnig, P., 2004. Anisotropic mechanical properties of tissue components in human atherosclerotic plaques. J. Biomech. Eng. 126, 657–65.

Iaizzo, P.A., 2013. Heart valves : from design to clinical implantation. Springer US.

Jánosi, R.A., Kahlert, P., Plicht, B., Wendt, D., Eggebrecht, H., Erbel, R., Buck, T., 2011. Measurement of the aortic annulus size by real-time three-dimensional transesophageal echocardiography. Minim. Invasive Ther. Allied Technol. 20, 85–94. https://doi.org/10.3109/13645706.2011.557385

Jilaihawi, H., Kashif, M., Fontana, G., Furugen, A., Shiota, T., Friede, G., Makhija, R., Doctor, N., Leon, M.B., Makkar, R.R., 2012. Cross-Sectional Computed Tomographic Assessment Improves Accuracy of Aortic Annular Sizing for Transcatheter Aortic Valve Replacement and Reduces the Incidence of Paravalvular Aortic Regurgitation. J. Am. Coll. Cardiol. 59, 1275–1286. https://doi.org/10.1016/j.jacc.2011.11.045

Jung, C., Lichtenauer, M., Figulla, H.-R., Wernly, B., Goebel, B., Foerster, M., Edlinger, C., Lauten, A., 2017. Microparticles in patients undergoing transcatheter aortic valve implantation (TAVI). Heart Vessels 32, 458–466. https://doi.org/10.1007/s00380-016-0885-z

Kalyana Sundaram, G.B., Balakrishnan, K.R., Kumar, R.K., 2015. Aortic valve dynamics using a fluid structure interaction model – The physiology of opening and closing. J.

Biomech. 48, 1737–1744. https://doi.org/10.1016/J.JBIOMECH.2015.05.012

Kandail, H.S., Trivedi, S.D., Shaikh, A.C., Bajwa, T.K., O'Hair, D.P., Jahangir, A., LaDisa, J.F., 2018. Impact of annular and supra-annular CoreValve deployment locations on aortic and coronary artery hemodynamics. J. Mech. Behav. Biomed. Mater. 86, 131–142. https://doi.org/10.1016/J.JMBBM.2018.06.032

Kappetein, A.P., Head, S.J., Genereux, P., Piazza, N., Van Mieghem, N.M., Blackstone, E.H., Brott, T.G., Cohen, D.J., Cutlip, D.E., van Es, G.-A., Hahn, R.T., Kirtane, A.J., Krucoff, M.W., Kodali, S., Mack, M.J., Mehran, R., Rodes-Cabau, J., Vranckx, P., Webb, J.G., Windecker, S., Serruys, P.W., Leon, M.B., Valve Academic Research Consortium (VARC)-2, 2012. Updated standardized endpoint definitions for transcatheter aortic valve implantation: the Valve Academic Research Consortium-2 consensus document (VARC-2). Eur. J. Cardio-Thoracic Surg. 42, S45–S60. https://doi.org/10.1093/ejcts/ezs533

Kasel, A.M., Cassese, S., Bleiziffer, S., Amaki, M., Hahn, R.T., Kastrati, A., Sengupta, P.P., 2013. Standardized Imaging for Aortic Annular Sizing. JACC Cardiovasc. Imaging 6, 249–262. https://doi.org/10.1016/j.jcmg.2012.12.005

Kempfert, J., Van Linden, A., Lehmkuhl, L., Rastan, A.J., Holzhey, D., Blumenstein, J., Mohr, F.W., Walther, T., 2012. Aortic annulus sizing: echocardiographic versus computed tomography derived measurements in comparison with direct surgical sizing. Eur. J. Cardio-Thoracic Surg. 42, 627–633. https://doi.org/10.1093/ejcts/ezs064

Kim, U., Blanke, P., Windecker, S., Kasel, A.M., Schäfer, U., Walters, D., Linke, A., Le Breton, H., Schymik, G., Spence, M.S., Søndergaard, L., Abdel-Wahab, M., Worthley, S., Tchétché, D., Reichenspurner, H., Ohana, M., Sellers, S.L., Leipsic, J.A., 2018. Computed tomography-based oversizing and incidence of paravalvular aortic regurgitation and permanent pacemaker implantation with a new-generation self-

expanding transcatheter heart valve. EuroIntervention 14, e511–e518. https://doi.org/10.4244/EIJ-D-17-01040

Kopanidis, A., Pantos, I., Alexopoulos, N., Theodorakakos, A., Efstathopoulos, E., Katritsis, D., 2015. Aortic Flow Patterns After Simulated Implantation of Transcatheter Aortic Valves. Hellenic J. Cardiol. 56, 418–28.

Le Couteulx, S., Caudron, J., Dubourg, B., Cauchois, G., Dupré, M., Michelin, P., Durand, E., Eltchaninoff, H., Dacher, J.-N., 2018. Multidetector computed tomography sizing of aortic annulus prior to transcatheter aortic valve replacement (TAVR): Variability and impact of observer experience. Diagn. Interv. Imaging 99, 279–289. https://doi.org/10.1016/J.DIII.2017.12.007

Lehmkuhl, L., Foldyna, B., Haensig, M., von Aspern, K., Lücke, C., Andres, C., Grothoff, M., Riese, F., Nitzsche, S., Holzhey, D., Linke, A., Mohr, F.-W., Gutberlet, M., 2013. Role of preprocedural computed tomography in transcatheter aortic valve implantation. Rofo 185, 941–9.

Luraghi, G., Migliavacca, F., García-González, A., Chiastra, C., Rossi, A., Cao, D., Stefanini, G., Rodriguez Matas, J.F., 2019. On the Modeling of Patient-Specific Transcatheter Aortic Valve Replacement: A Fluid-Structure Interaction Approach. Cardiovasc. Eng. Technol. https://doi.org/10.1007/s13239-019-00427-0

Luraghi, G., Migliavacca, F., Rodriguez Matas, J.F., 2018. Study on the Accuracy of Structural and FSI Heart Valves Simulations. Cardiovasc. Eng. Technol. 9, 1–16. https://doi.org/10.1007/s13239-018-00373-3

Luraghi, G., Wu, W., De Gaetano, F., Rodriguez Matas, J.F., Moggridge, G.D., Serrani, M., Stasiak, J., Costantino, M.L., Migliavacca, F., 2017. Evaluation of an aortic valve prosthesis: Fluid-structure interaction or structural simulation? J. Biomech. 58, 45–51. https://doi.org/10.1016/j.jbiomech.2017.04.004

Maleki, H., Shahriari, S., Labrosse, M., Rodés-Cabau, J., Pibarot, P., Kadem, L., 2015. Effect of Aortic Annulus Size and Prosthesis Oversizing on the Hemodynamics and Leaflet Bending Stress of Transcatheter Valves: An In Vitro Study. Can. J. Cardiol. 31, 1041–1046. https://doi.org/10.1016/j.cjca.2015.03.026

Mao, W., Wang, Q., Kodali, S., Sun, W., 2018. Numerical Parametric Study of Paravalvular Leak Following a Transcatheter Aortic Valve Deployment Into a Patient-Specific Aortic Root. J. Biomech. Eng. 140, 101007. https://doi.org/10.1115/1.4040457

Morganti, S., Conti, M., Aiello, M., Valentini, A., Mazzola, A., Reali, A., Auricchio, F., 2014. Simulation of transcatheter aortic valve implantation through patient-specific finite element analysis: Two clinical cases. J. Biomech. 47, 2547–2555. https://doi.org/10.1016/j.jbiomech.2014.06.007

O'Brien, B., Schoenhagen, P., Kapadia, S.R., Svensson, L.G., Rodriguez, L., Griffin, B.P., Tuzcu, E.M., Desai, M.Y., 2011. Integration of 3D imaging data in the assessment of aortic stenosis: impact on classification of disease severity. Circ. Cardiovasc. Imaging 4, 566–73. https://doi.org/10.1161/CIRCIMAGING.111.964916

Ovcharenko, E.A., Klyshnikov, K.U., Yuzhalin, A.E., Savrasov, G.V., Kokov, A.N., Batranin, A.V., Ganyukov, V.I., Kudryavtseva, Y.A., 2016. Modeling of transcatheter aortic valve replacement: Patient specific vs general approaches based on finite element analysis. Comput. Biol. Med. 69, 29–36. https://doi.org/10.1016/j.compbiomed.2015.12.001

Ranga, A., Mongrain, R., Galaz, R.M., Biadillah, Y., Cartier, R., 2004. Large-displacement 3D structural analysis of an aortic valve model with nonlinear material properties. J. Med. Eng. Technol. 28, 95–103. https://doi.org/10.1080/0309190042000193847

Russ, C., Hopf, R., Hirsch, S., Sundermann, S., Falk, V., Szekely, G., Gessat, M., 2013. Simulation of transcatheter aortic valve implantation under consideration of leaflet

calcification, in: 2013 35th Annual International Conference of the IEEE Engineering in Medicine and Biology Society (EMBC). IEEE, pp. 711–714. https://doi.org/10.1109/EMBC.2013.6609599

Schoenhagen, P., Numburi, U., Halliburton, S.S., Aulbach, P., von Roden, M., Desai, M.Y., Rodriguez, L.L., Kapadia, S.R., Tuzcu, E.M., Lytle, B.W., 2010. Three-dimensional imaging in the context of minimally invasive and transcatheter cardiovascular interventions using multi-detector computed tomography: from pre-operative planning to intra-operative guidance. Eur. Heart J. 31, 2727–2740. https://doi.org/10.1093/eurheartj/ehq302

Smith, C.R., Leon, M.B., Mack, M.J., Miller, D.C., Moses, J.W., Svensson, L.G., Tuzcu, E.M., Webb, J.G., Fontana, G.P., Makkar, R.R., Williams, M., Dewey, T., Kapadia, S., Babaliaros, V., Thourani, V.H., Corso, P., Pichard, A.D., Bavaria, J.E., Herrmann, H.C., Akin, J.J., Anderson, W.N., Wang, D., Pocock, S.J., PARTNER Trial Investigators, 2011. Transcatheter versus surgical aortic-valve replacement in high-risk patients. N. Engl. J. Med. 364, 2187–98. https://doi.org/10.1056/NEJMoa1103510

Spühler, J.H., Jansson, J., Jansson, N., Hoffman, J., 2018. 3D Fluid-Structure Interaction Simulation of Aortic Valves Using a Unified Continuum ALE FEM Model. Front. Physiol. 9, 363. https://doi.org/10.3389/fphys.2018.00363

Sturla, F., Votta, E., Stevanella, M., Conti, C.A., Redaelli, A., 2013. Impact of modeling fluid–structure interaction in the computational analysis of aortic root biomechanics. Med. Eng. Phys. 35, 1721–1730. https://doi.org/10.1016/J.MEDENGPHY.2013.07.015

Toma, M., Jensen, M.Ø., Einstein, D.R., Yoganathan, A.P., Cochran, R.P., Kunzelman, K.S., 2016. Fluid–Structure Interaction Analysis of Papillary Muscle Forces Using a Comprehensive Mitral Valve Model with 3D Chordal Structure. Ann. Biomed. Eng. 44, 942–953. https://doi.org/10.1007/s10439-015-1385-5

Vande Geest, J.P., Sacks, M.S., Vorp, D.A., 2006. The effects of aneurysm on the biaxial mechanical behavior of human abdominal aorta. J. Biomech. 39, 1324–1334. https://doi.org/10.1016/j.jbiomech.2005.03.003

Vy, P., Auffret, V., Badel, P., Rochette, M., Le Breton, H., Haigron, P., Avril, S., 2016. Review of patient-specific simulations of transcatheter aortic valve implantation. Int. J. Adv. Eng. Sci. Appl. Math. 8, 2–24. https://doi.org/10.1007/s12572-015-0139-9

Wu, W., Pott, D., Mazza, B., Sironi, T., Dordoni, E., Chiastra, C., Petrini, L., Pennati, G., Dubini, G., Steinseifer, U., Sonntag, S., Kuetting, M., Migliavacca, F., 2016a. Fluid–Structure Interaction Model of a Percutaneous Aortic Valve: Comparison with an In Vitro Test and Feasibility Study in a Patient-Specific Case. Ann. Biomed. Eng. 44, 590–603. https://doi.org/10.1007/s10439-015-1429-x

Wu, W., Pott, D., Mazza, B., Sironi, T., Dordoni, E., Chiastra, C., Petrini, L., Pennati, G., Dubini, G., Steinseifer, U., Sonntag, S.J., Kuetting, M., Migliavacca, F., 2016b. Fluid–Structure Interaction Model of a Percutaneous Aortic Valve: Comparison with an In Vitro Test and Feasibility Study in a Patient-Specific Case. Ann. Biomed. Eng. 44, 590–603. https://doi.org/10.1007/s10439-015-1429-x

Figures

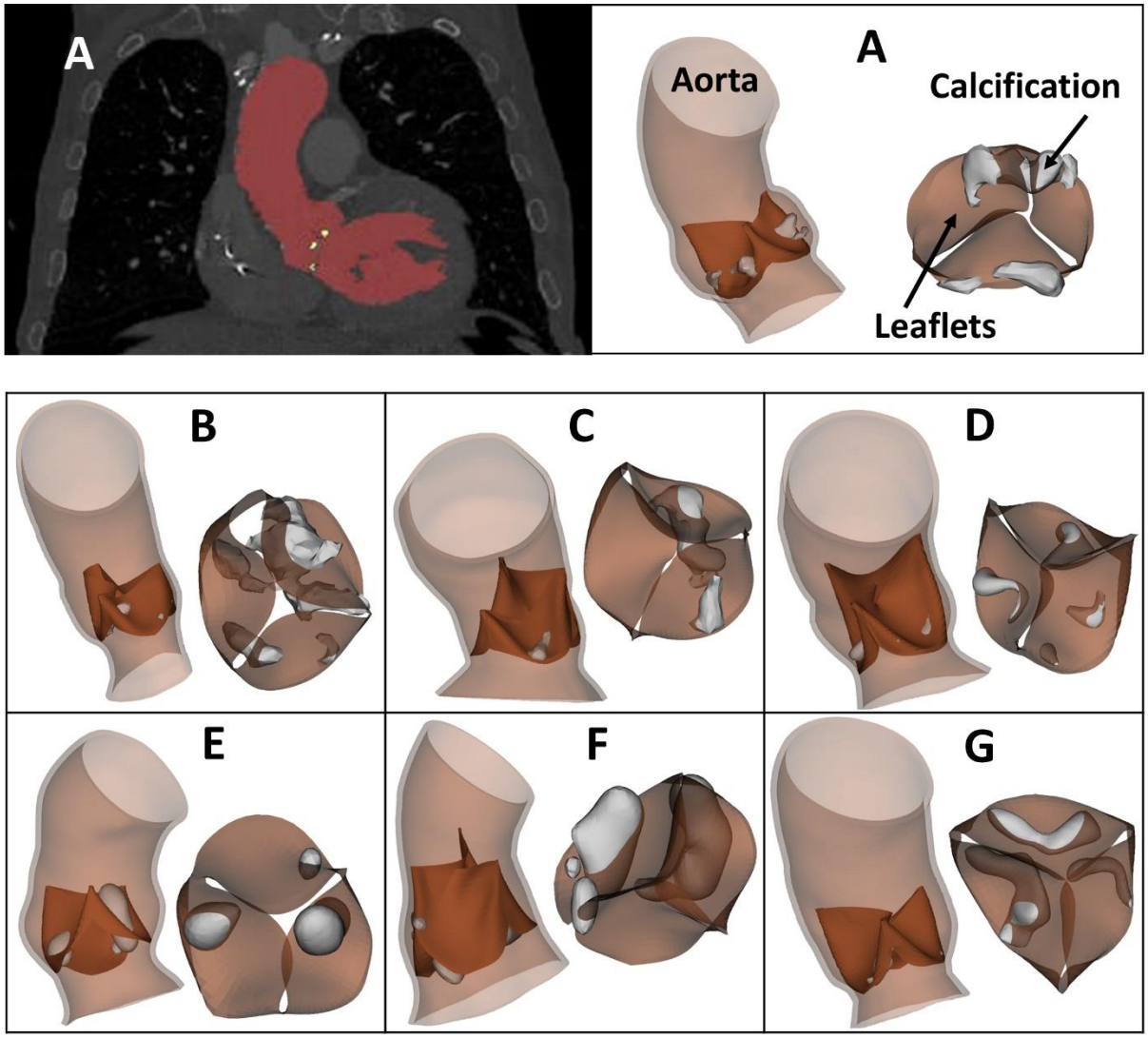

Fig 1 - Top panels: example of segmented CT image and reconstructed geometries of aorta, native valve with native leaflets and calcification for patient A. Bottom panels: reconstructed geometries of all the other patients (from B to G).

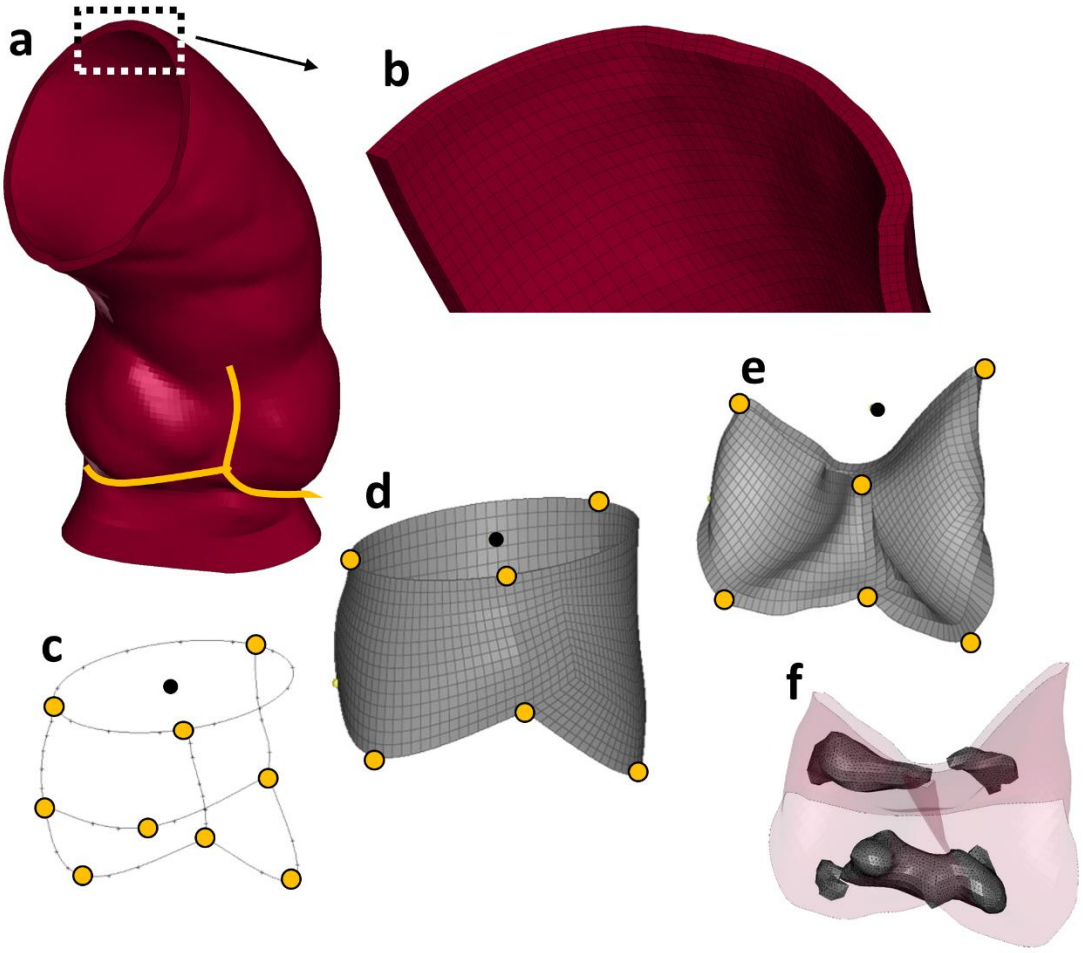

Fig 2 –Segmented surface of the aortic lumen (a), which was extruded with a constant thickness and meshed with hexahedral solid elements (b); reference points (yellow points) to draw the surfaces of the valve considering the free margin as a circular arc (whose center is the black point) (c); quadrilateral elements of the valve (d) and its end-diastole configuration (e); surface-to-surface tied contact between the calcifications and the valve (f).

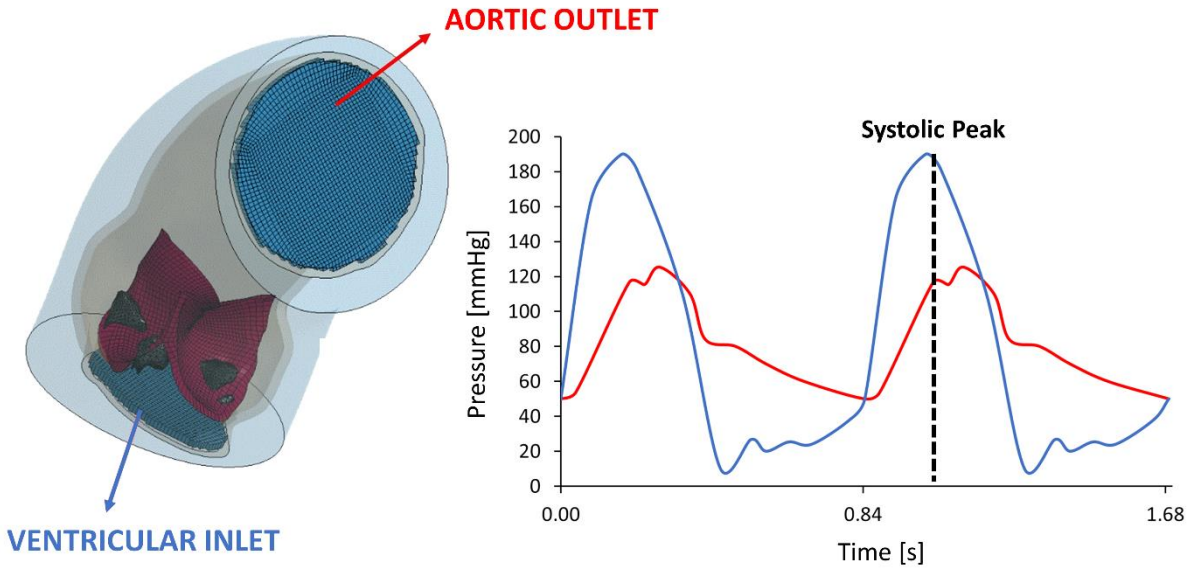

Fig 3 - Left panel: Aortic root model for the FSI simulation, in which the patient-specific domain is immersed in the fluid domain. Right panel: the ventricular inlet and aortic outlet are shown with ventricular and aortic pressures used as boundary conditions (the actual curves of patient B are shown).

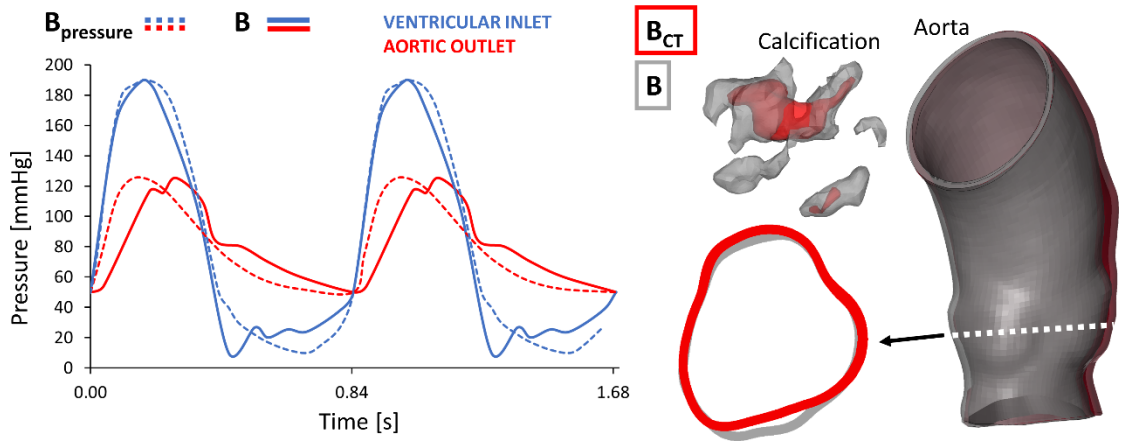

Fig 4 - Left panel: actual pressure curves of patient B (solid lines) and physiological waveforms scaled with the patient maximum and minimum pressure values applied in model $B_{pressure}$ (dotted lines). Right panel: calification and aorta geometries of patient B reconstructed from real CT scans with 0.6 mm of slice thickness (in gray) and with 2.4 mm of slice thickness (model B_{CT}, in red).

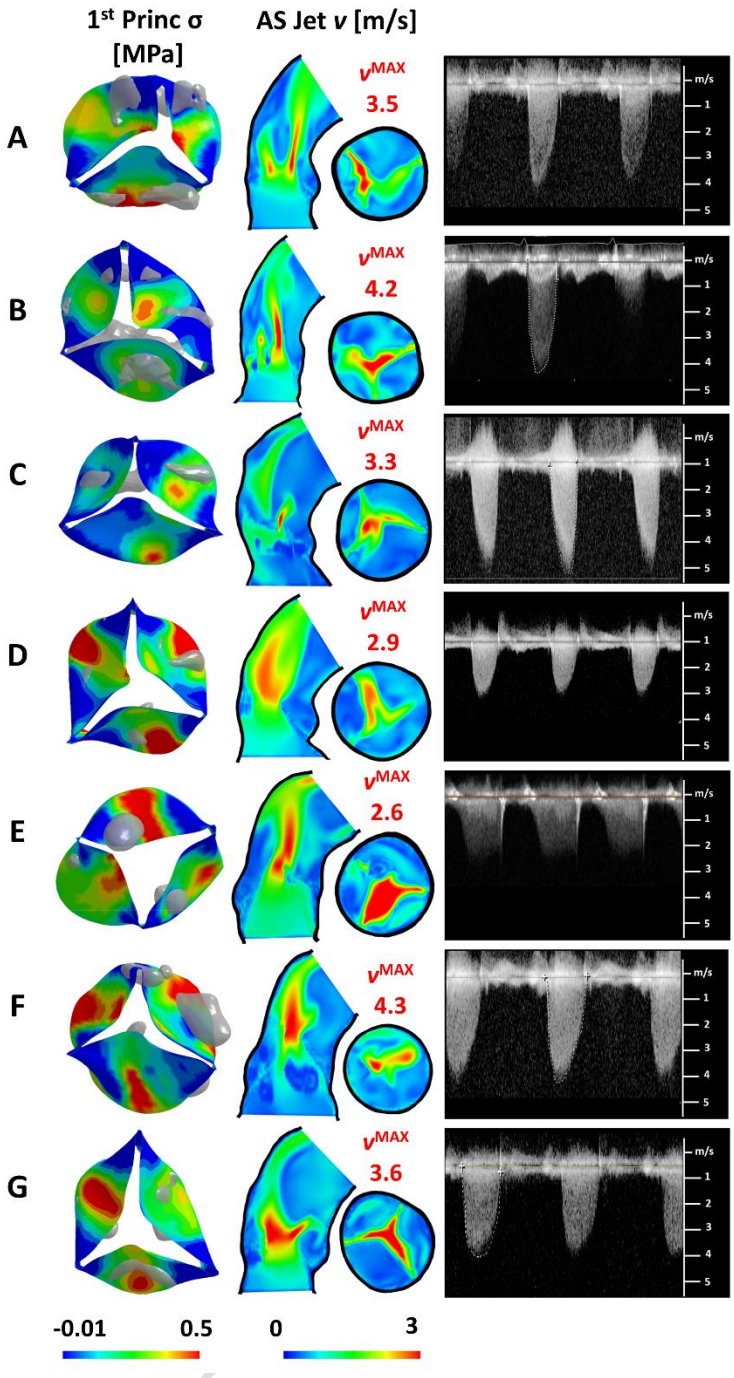

Fig 5 - Left panels: aortic valve configuration at peak systolic pressure for the seven patients showing the 1st principal stress field on the leaflets. Central panels: velocity field on longitudinal and transversal sections of the aorta. Right panels: Doppler tracings for the seven investigated patients.

Tables

Table 1: Aortic stenosis (AS) jet velocity, mean pressure gradient(ΔP), calculated using Eq. (1), and effective orifice area (EOA) estimated from transthoracic Doppler echocardiography (TTE) for each patient according to Eq. (2).

Patient	AS jet v [m/s]	ΔP [mmHg]	EOA [cm^2]
A	4.2	42	0.88
B	4.6	46	0.7
C	5.4	77	0.65
D	3.2	28	0.8
E	3.2	50	0.7
F	4.6	47	0.7
G	4.1	47	0.8

Table 2: Pixel spacing and slice thickness of the CT scans and estimated aortic valve annulus for each patient

Patient	Pixel Spacing [mm^2]	Slice Thickness [mm]	Aortic valve annulus [mm]
A	0.703 x 0.703	0.6	21x29
B	0.703 x 0.703	0.6	21x29
C	0.816 x 0.816	3.0	22.3
D	0.703 x 0.703	0.6	21x28
E	0.703 x 0.703	0.6	21x28
F	0.816 x 0.816	3.0	21
G	0.703 x 0.703	0.6	20x25

Table 3: Aortic and ventricular pressure values (max/min) and heart rate for each rate.

Patient	Aortic pressure [mmHg]	Ventricular pressure [mmHg]	Heart rate [bmp]
A	123/70	169/20	84
B*	126/50	191/36	71
C	116/80	157/63	65
D	136/74	163/10	74
E	114/63	153/65	70
F	143/69	190/20	64
G	98/58	158/22	73

* Patient with temporal pressure tracings

Table 4: Comparison between clinical data and results of the models in terms of aortic valve annulus, geometric orifice area (GOA) ad aortic stenosis (AS) jet velocity. Results from sensitivity of data quality models are also reported.

Patient	Aortic valve annulus [mm]		GOA [cm^2]		AS Jet velocity [m/s]	
	Clinical data	Segmentation	Clinical data	FSI Model	Clinical data	FSI Model
A	21x29	26.4	1.26	1.31	4.2	3.5
B	21x29	25	1	1.01	4.6	4.2
$B_{pressure}$	21x29	25	1	0.98	4.6	4.1
B_{CT}	21x29	22.7	1	0.86	4.6	3.4
C	22.3	29.8	0.93	1.01	5.4	3.3
D	21x28	29.1	1.14	1.21	3.2	2.9
E	21x28	29.6	1	1.17	3.2	2.6
F	21	31.9	1	1.01	4.6	4.3
G	20x25	23.5	1.14	1.15	4.1	3.6